



Onion-like carbon-modified TiO₂ coating by suspension plasma spray with enhanced photocatalytic performances

Yaoyao Fu · Yi Liu · Hua Li

Received: 28 March 2019 / Accepted: 8 August 2019
© Springer Nature B.V. 2019

Abstract Onion-like carbon (OLC), a novel carbonaceous nanomaterial, has already attracted widespread concern due to its exceptional physicochemical properties. In this work, OLC nanoparticles (5–10 nm in diameter) were used as additives to fabricate nanotitania (TiO₂) coatings by suspension plasma spray (SPS) for photocatalytic degrading methylene blue. The starting microstructure and chemistry of both OLC and TiO₂ nanoparticles were retained after deposition process, and homogeneous dispersion of OLC in the coating was detected, which indicates SPS is an alternative and efficient technique to fabricate semiconductor-carbonaceous nanomaterials coatings. The new TiO₂-OLC composite shows typical mesoporous structure. And aligned interfacial bond of OLC spheres with the (101) plane of anatase crystals was revealed. TiO₂-OLC shows enhanced activity of degrading methylene blue under both UV and visible light irradiation than pure TiO₂ coating. We have elucidated the enhancement mechanism from three aspects, namely, reduction of the bandgap, minimization of photo-induced-carriers

recombination, and promotion of adsorption capacity for methylene blue.

Keywords Titania coating · Onion-like carbon · Nanoparticles · Suspension plasma spray · Photocatalytic performances · Nanocomposites

Introduction

Onion-like carbon (OLC), also named as multi-shell fullerene (Ugarte 1992), is structured by concentric shells of carbon atoms with a 0.34-nm distance between adjacent carbon shells. Despite similar discovery time to C₆₀/carbon nanotube and much earlier time than graphene, OLC has received the slightest concern among the carbonaceous nanomaterials in both laboratory and industry due to fabrication difficulties and inadequate practical applications. Booming efforts on practical research of OLC were seen until OLC particles were synthesized in large scale by heat-treating detonation nanodiamonds (Kuznetsov et al. 1994). Owing to excellent physicochemical properties such as modifiable surface chemistry, perfect sphericity, good electrical conductivity, and low cytotoxicity, nanodiamond-derived OLC has been extensively explored for potential applications for electrochemical energy storage (Zeiger et al. 2016), solid lubrication (Berman et al. 2018), and biomedicine (Ghosh et al. 2011). However, there are still challenges in how to properly modify OLC particles to achieve the desired performance.

Y. Fu · Y. Liu · H. Li (✉)
Key Laboratory of Marine Materials and Related Technologies,
Zhejiang Key Laboratory of Marine Materials and Protective
Technologies, Ningbo Institute of Materials Technology and
Engineering, Chinese Academy of Sciences, Ningbo 315201,
China
e-mail: lihua@nimte.ac.cn

Y. Fu
Center of Materials Science and Optoelectronics Engineering,
University of Chinese Academy of Sciences, Beijing 100049,
China

Among the oxide photocatalyst, titania (TiO_2) is the most widely implemented photocatalyst. However, unmodified TiO_2 performs unsatisfactorily because of its wide bandgap width, rapid recombination rate of the photo-induced carriers (Liu et al. 2014; Schneider et al. 2014). Tremendous and continuous efforts have been attempted to reinforce the photocatalytic efficiency of bare TiO_2 through a variety of techniques, such as element doping (Boningari et al. 2018; Feng et al. 2018), dye sensitization (Wang and Lang 2018), metal/metal oxide nanoparticle loading (Sakthivel et al. 2004; Zhang et al. 2010b), and construction of heterojunctions (Chen et al. 2018; Correia et al. 2018; Hao et al. 2017). As an alternative strategy, synthesizing TiO_2 -carbonaceous nanomaterials composites has attracted considerable attention for achieving enhanced photocatalysis reactions (Leary and Westwood 2011; Li et al. 2016; Nalid et al. 2017; Wang et al. 2017; Woan et al. 2009), which usually involve three major processes, namely photons absorption to create electron-hole pairs, separation and migration/recombination of the photo-induced electron-hole pairs, and photocatalytic reaction on the photocatalyst surface. Graphene (Lee et al. 2012; Ton et al. 2018; Zhang et al. 2010d), carbon nanotube (Li et al. 2018; Shaban et al. 2018; Woan et al. 2009), and other carbonaceous nanomaterials have been proven to be effective in enhancing the photocatalytic performances of TiO_2 .

To date, several fundamental regimes accounting for the enhanced photocatalytic activity of TiO_2 by incorporating carbonaceous nanomaterials have been proposed (Leary and Westwood 2011). Among these mechanisms, decreased bandgap, reduced charge-carrier recombination rate, and promoted adsorption of reactants on the photocatalyst surface play the predominate roles. OLC nanoparticles were proven to have excellent physicochemical properties, such as high adsorption ability (Sakulthaew et al. 2015) and electrical conductivity (Zeiger et al. 2015). They might be a good candidate as additives to enhance photocatalytic performances of TiO_2 (Leary and Westwood 2011). However, to the best knowledge of the authors, publication on use of OLC for enhancing TiO_2 photocatalytic activity has not been seen.

To fabricate TiO_2 -carbonaceous nanomaterials composites, selecting appropriate processing techniques is one of the essential considerations. In previous studies, the composites have been fabricated by a variety of techniques such as hydrothermal processing

(Rajagopal and Ryu 2018; Zhang et al. 2010a), sol-gel (Re et al. 2018; Zhang et al. 2010c), and CVD (Fitri et al. 2017; Liu et al. 2018). Apart from their capability of making controllable structures for favorable performances; however, the abovementioned techniques bear the shortcomings relating to separation and regeneration of TiO_2 powder after photocatalytic reaction (Fitri et al. 2017; Liu et al. 2018; Rajagopal and Ryu 2018; Zhang et al. 2010a), low processing efficiency (Rajagopal and Ryu 2018; Re et al. 2018; Zhang et al. 2010a, c), and difficulties in large scale production. Since the photocatalytic reactions usually occur at the very thin top layer of TiO_2 -based composites, to avoid secondary pollution resulted from released nanoparticles, film or coating might be the best form of the photocatalyst. Herein, suspension plasma spray (SPS), which has shown promising capabilities in overcoming the aggregation of nanoparticles during atmospheric plasma spraying (Pawlowski 2009), would be suitable for depositing the nanostructured TiO_2 coatings. During the spraying process, evaporation of suspension liquid could result in reaction temperature decrease, which would facilitate the retention of the intrinsic physicochemical properties of starting nanoparticles (Bannier et al. 2011; Robinson et al. 2015; Toma et al. 2006a; Tomaszek et al. 2006).

In this paper, TiO_2 -OLC composite coatings were fabricated by SPS using TiO_2 and OLC nanoparticles as the starting nanomaterials. Nanostructured features of OLC and TiO_2 particles were retained in the coatings and unique dispersion of the OLC particles in the coatings was achieved. It was surprisingly noted that addition of OLC nanoparticles enhanced the photocatalytic performances of the pure TiO_2 . The synergistic effect of OLC and TiO_2 particles was further elaborated.

Materials and methods

Suspension preparation

Degussa P25 and nanodiamond-derived OLC nanoparticles were used as the starting materials. The TiO_2 nanoparticles are composed of 80.77 vol.% anatase and 19.23 vol.% rutile, and the TiO_2 nanoparticles tend to agglomerate in microscale clusters (Fig. 1a). The starting OLC nanoparticles (Nafortis Co. Ltd., China) show the size of 5–10 nm in diameter with typical concentric carbon atoms rings, and the spacing of

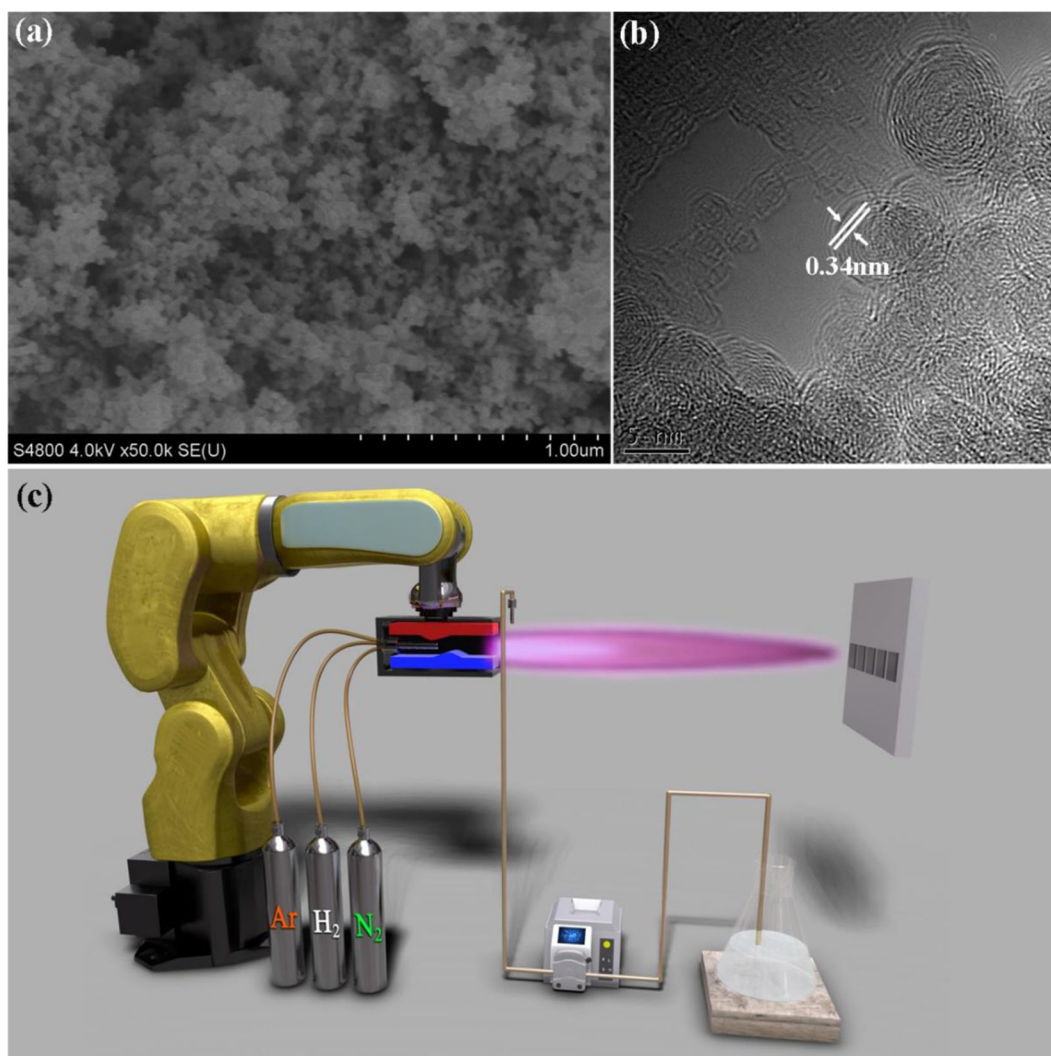


Fig. 1 Morphology of the starting TiO₂ (a) and the OLC nanoparticles (b) and schematic diagram of suspension plasma spraying (SPS) apparatus (c)

0.34 nm between successive cages can be clearly recognized (Fig. 1b). Deionized water and ethanol were used as solvents for preparing the suspensions, and polyvinylpyrrolidone (PVP) was used as the dispersing agent. For the suspension preparation, 10 g TiO₂ was dispersed in 100 ml deionized water, and 4 g PVP was dissolved in 100 ml ethanol. Both the solutions were then mixed and kept stirred for entire mixing. To prepare TiO₂-OLC binary suspension, ultrasonic dispersion of 1 g OLC in 100 ml distilled water was carried out, followed by additional dispersion of 9 g TiO₂ in the suspension. The suspension was then mixed with the 100 ml ethanol solution containing 4 g PVP, further

vigorous stirring was conducted for the solution to be used as the feedstock suspension for coating fabrication.

Coating fabrication by suspension plasma spray

TiO₂ and TiO₂-OLC binary suspensions were sprayed using a plasma spray system (XM-80SK, Shanghai, China), and a homemade automatic feeding apparatus was employed for delivering the liquid feedstock. The continuously stirred suspension was fed into the plasma torch by a peristaltic pump, ensuring both atomization and radial injection of the droplets into plasma torch. The plasma power of 25 kW was used for the coating

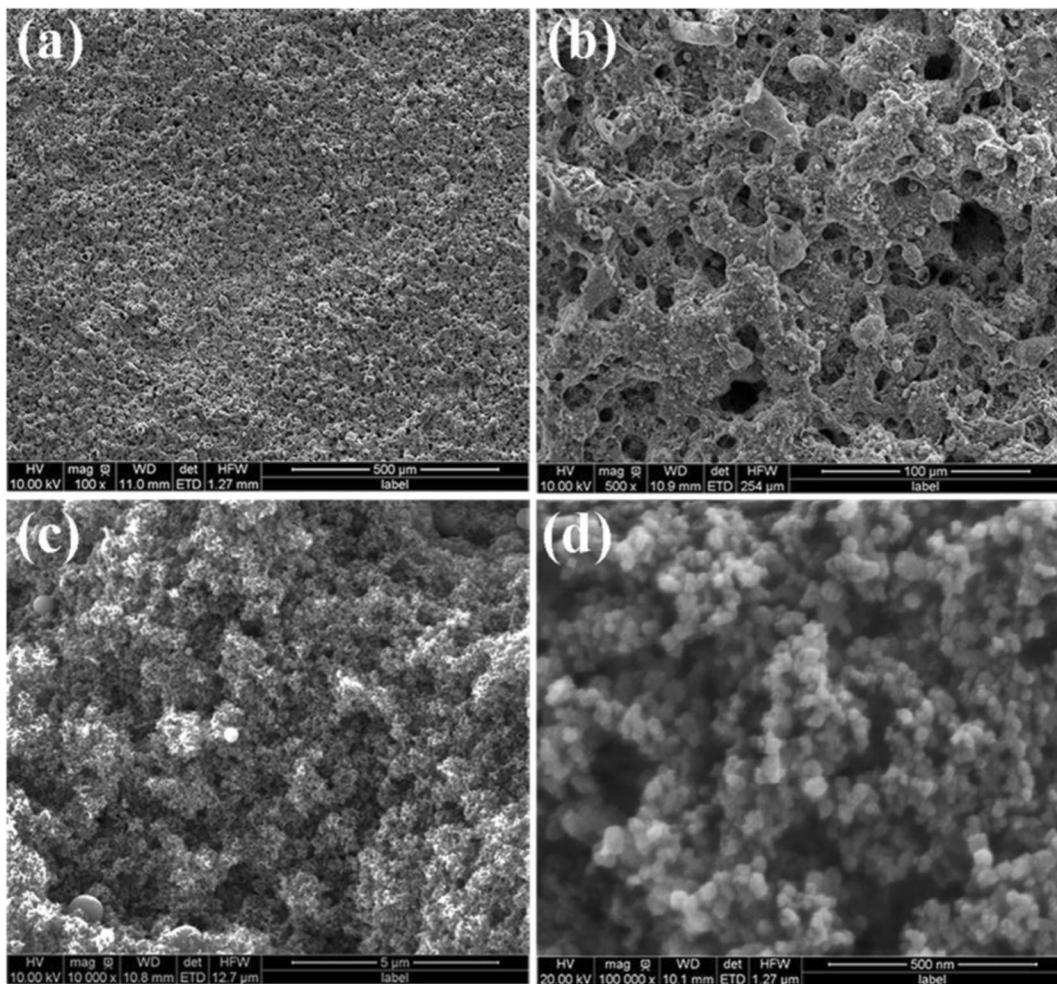


Fig. 2 FESEM images of the as-sprayed coatings, **a, b** porous topographical morphologies, and **c, d** enlarged topographical views showing well retained TiO_2 nanoparticles in the coatings

deposition. Pressure of the primary gas (Ar) and the auxiliary gas (H_2) was 0.7 MPa and 0.3 MPa, respectively. The spray distance was 80 mm. Stainless steel plates with the dimension of $200 \times 200 \times 3$ mm were used as substrates, which were degreased and sand-blasted with alumina grits prior to the spraying. Figure 1 c gives the schematic diagram of suspension plasma spraying (SPS) in the research.

Microstructural characterization

Microstructure of the starting nanoparticles and the as-sprayed coatings was characterized by field emission scanning electron microscopy (FE-SEM, Quanta FEG 250, USA). Chemistry of the samples was examined by X-ray diffraction (XRD, Bruker D8 Advance Davinci,

Germany) using $\text{Cu K}\alpha$ radiation ($\lambda = 1.54 \text{ \AA}$) operated at 40 mA and 40 kV. From the XRD spectra, quantification of the phases was carried out by integrating and comparing the anatase (101) and rutile (110) peaks using the equation: $C_A = 8I_A / (8I_A + 13I_R)$, where C_A is the phase content of anatase, I_A and I_R are the relative peak intensities of anatase (101) and rutile (110) (Robinson et al. 2015). Furthermore, the Scherrer equation was used to estimate the crystallite size following the equation: $D = K\lambda / (\beta \cos\theta)$, where D is the crystallite size, K is the shape factor (0.9), λ is the X-ray wavelength (0.154 nm in this case), β is the full width in radians at half maximum of the peak, and θ is the Bragg diffraction angle in degree (Robinson et al. 2015). Raman spectroscopy was performed using a Renishaw Raman microscope, measuring in the wavenumber range from 100 to

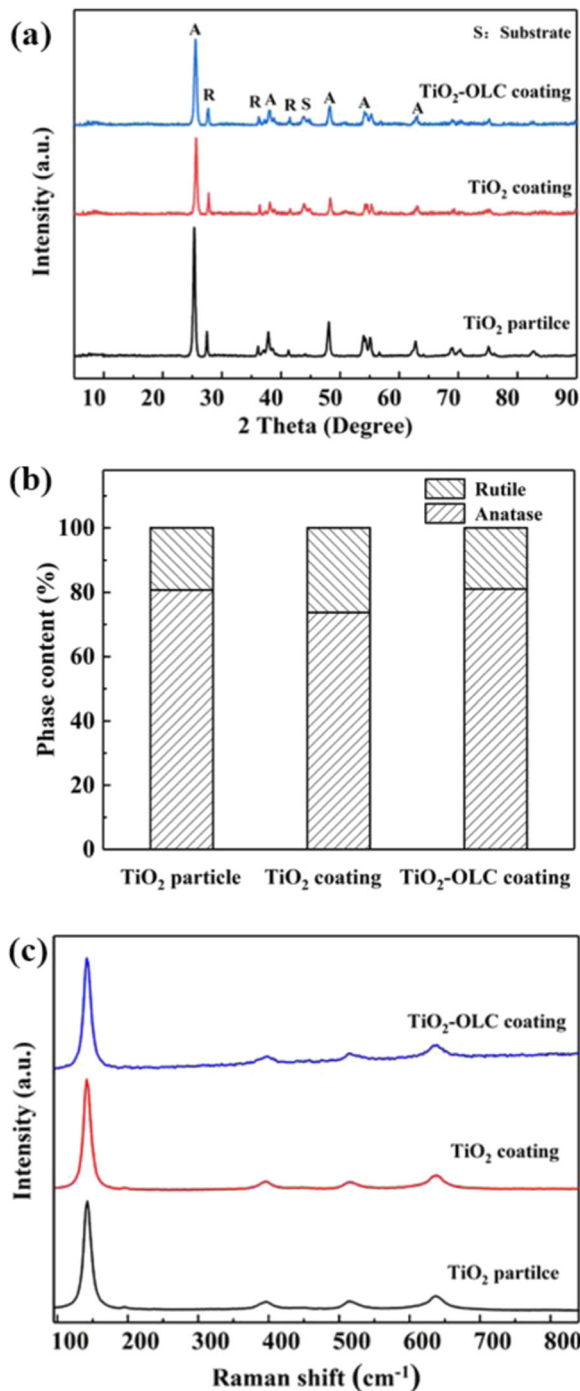


Fig. 3 XRD spectra (a) and calculated phase content (b) of the samples and Raman spectra of the samples (c)

1000 cm⁻¹. And photoluminescence (PL) spectra were also recorded using Renishaw Raman microscope under 325 nm excitation at room temperature. High-resolution transmission electron microscopy (HRTEM) and

selected area electron diffraction (SAED) (FEI Tecnai F20, USA) characterization were also performed to further examine the interfaces between TiO₂ and OLC particles in the as-sprayed coatings. Chemistry of the samples was further assessed using the UV–Vis spectroscopy (PerkinElmer, Lambda 950, USA), and adsorption intensity-wavelength curves in reflectance mode between 200 and 800 nm were acquired. To calculate the bandwidth of the starting nanoparticles and the coatings, the reflectance spectra were converted to absorption curves according to the Kubelka-Munk (K-M) function, and then the optical band gap was derived from the Tauc equation (Ton et al. 2018).

Assessment of the dark reaction and photocatalytic activities

For the photocatalytic degradation testing, the coatings samples were immersed in 20 ml 5 ppm methylene blue (MB) solution. To achieve adsorption equilibrium between the coatings and the solution, the coatings were kept in the solution without light radiation for 1 h prior to the testing. The concentration of residual MB in the tested solution was recorded hourly by the microplate reader (Spectra Max 190, MD, USA) operated using 644 nm wavelength.

Results and discussion

Porous coating formation

According to the principle and requirement of the SPS technology, a plasma spraying system with controlling and feeding subsystem has been developed, in which the reactant gas flow, moving track, plasma gun speed, and feeding rate of the suspension could be regulated. The plasma was obtained from argon–hydrogen gases mixtures at a power intensity of about 25 kW. With the stimulation of current and voltage, the reactant gas would be motivated to be plasma, which heat the feedstock and trigger the following reactions. It was well established that suspension feedstock usually experiences three main steps during the SPS processing (Pawlowski 2009; Toma et al. 2006a, b), namely fragmentation and atomization of the injected drops, evaporation of the solvent

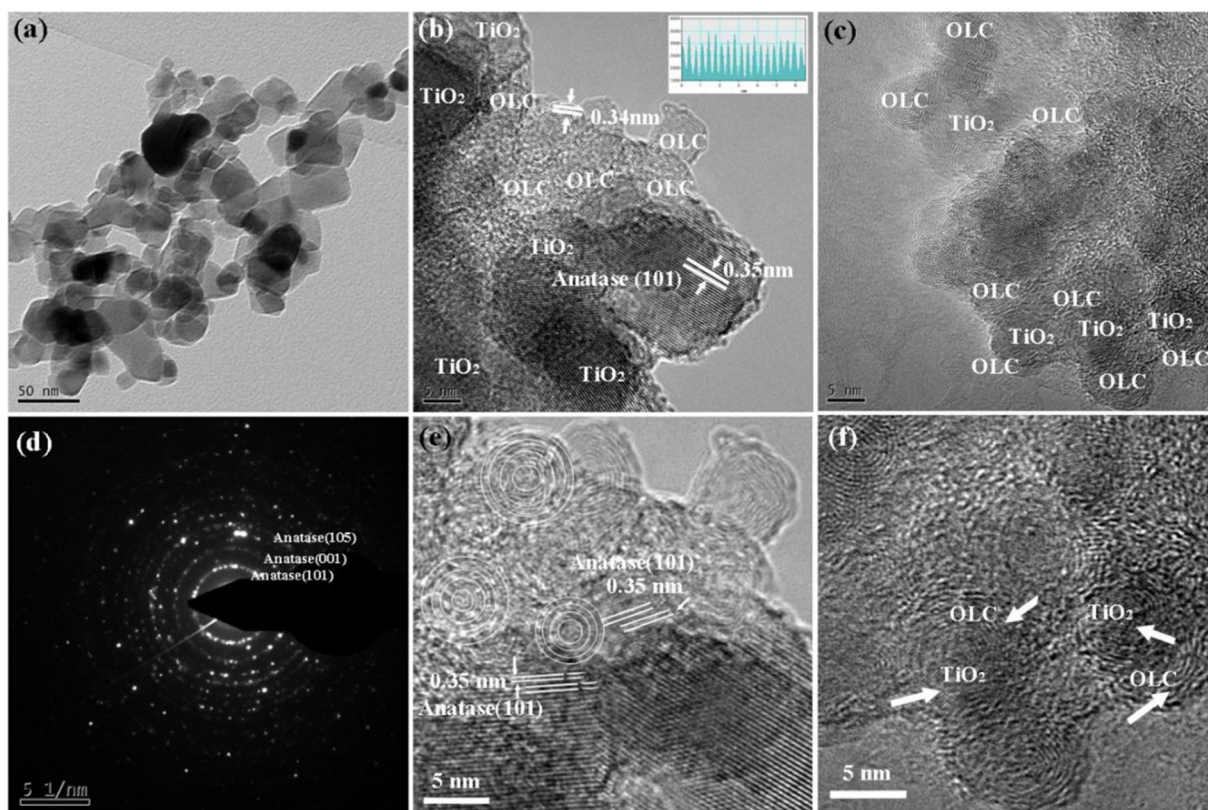


Fig. 4 TEM/HRTEM (a, b, c, e, f) and SAED (d) images of the as sprayed TiO_2 -OLC coating showing unique dispersion of OLC nanoparticles in the coating

and decomposition of PVP, and impact of the nanoparticles and coating formation.

In this case, both pure TiO_2 and TiO_2 -OLC coating were successfully fabricated, and porous structure was clearly seen from the surface SEM images of the coatings (Fig. 2a, b). This porous microstructural feature was believed to be caused predominately by the decomposition of PVP during the SPS heating processing (Ren et al. 2015). Porous structure is essentially required for photocatalytic materials to achieve enhanced activities. It seems that the characteristics of the original TiO_2 nanoparticles were mostly retained after the coating deposition (Fig. 2c, d). Being different from the typical lamellar structure of atmospheric plasma sprayed (APS) coatings, the SPS coatings show a granular structure. This could be explained by the phenomena that the nanoparticles were not fully melted during the SPS processing, due to the low processing temperature caused by evaporation of the solvent (Toma et al. 2006a).

Phase and microstructure

The commercial Degussa P25 has favorable photocatalytic efficiency, due to the synergic interaction of anatase (80%) and rutile (20%), and has been widely used as thermal spray feedstock for coating deposition (Kho et al. 2010). It is generally believed that, during the suspension plasma spraying, plasma power is already adequate for evaporating the liquid but still moderate for retaining the chemistry of starting TiO_2 particles (Toma et al. 2006c). The as-sprayed coating and primary P25 particles show similar strong diffraction peaks at 2θ of 25.28 [101], 37.8 [004], 48.05 [200], 53.89 [105], 55.1 [211], 62.6 [204], 68.7 [116], 70.3 [220], and 75.01 [215] that represent the crystalline phases of anatase and 27.44 [110], 36.09 [101], 39.20 [200], 41.25 [111], 44.05 [210], 56.04 [220], 64.06 [310], 69.02 [301], and 69.83 [112] that represent the crystalline phases of rutile, respectively (Fig. 3a). Further phase content calculation evidenced that anatase/rutile ratio kept unchanged after the coating fabrication (Fig. 3b),

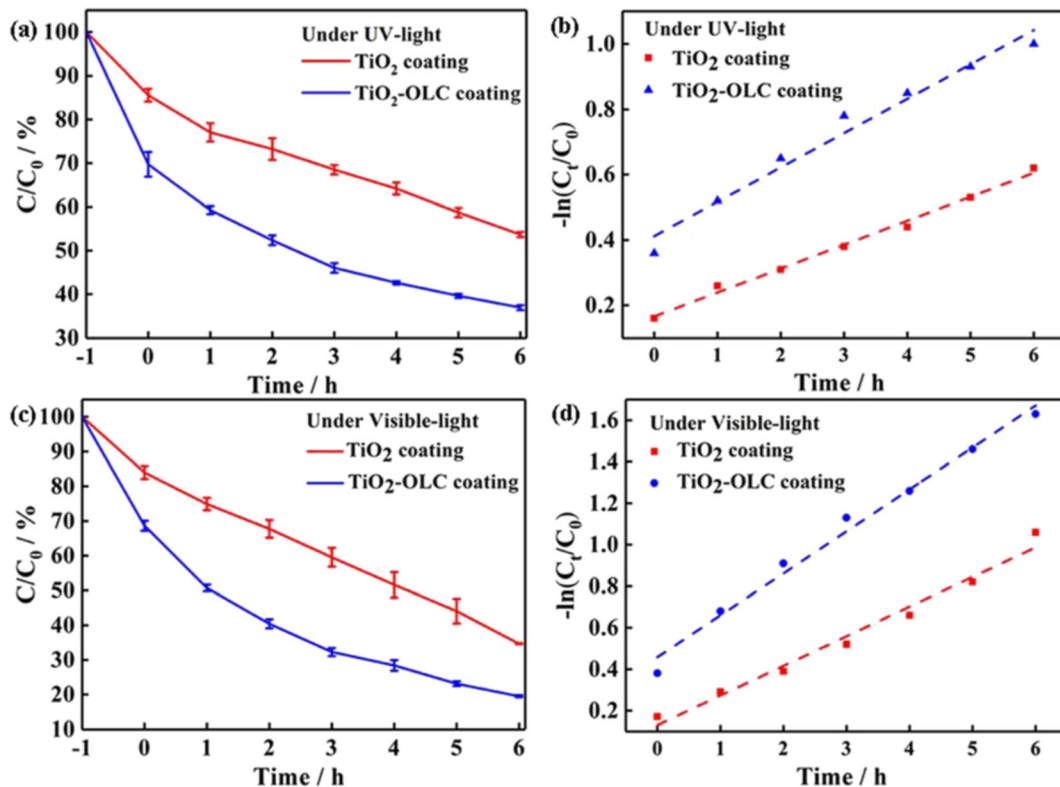


Fig. 5 Photocatalytic degradation of methylene blue under the illumination of UV-light (a, b) and visible light (c, d)

indicating appropriateness of the SPS processing route for fabricating TiO₂ coatings with desired phase composition. Meanwhile, the Raman spectrum of the P25 particle and as-fabricated composites shows consistent peaks (Fig. 3c), which further verifies the maintained phase of the P25 particle after coating process.

The as-sprayed TiO₂-OLC was further characterized by high-resolution transmission electron microscopy (HRTEM) and selected area electron diffraction (SAED) (Fig. 4). TiO₂ nanoparticles with original nanoscale are clearly seen in the coatings (Fig. 4a), which is consistent with the SEM observation (Fig. 2d). Meanwhile, the SAED (Fig. 4d) result verifies the XRD spectrum (Fig. 3a). Further magnified view showed unique dispersion of the OLC nanoparticles in the coatings, and interfacial bond of OLC spheres with the (101) plane of anatase crystals was recognized (Fig. 4b, e). The interface between anatase crystal and OLC particles is clearly seen. These structural features might influence the light-induced electron-hole pair formation behavior for tuned photocatalytic performances of TiO₂. The presence of OLC on the surface of TiO₂ particles would likely facilitate the adsorption of targeting organics for

efficient photocatalysis reaction process (Rajagopal and Ryu 2018).

Enhanced photocatalytic performance

Photocatalytic activity of the as-sprayed TiO₂ and the OLC-containing TiO₂ coating was examined by measuring degradation of dye methylene blue under both UV and visible light. The concentration variation of methylene blue with irradiation time is shown in Fig. 5. The result indicated that under both UV (Fig. 5a, b) and visible light (Fig. 5c, d) irradiations, the OLC-containing coating performed better than the pure TiO₂. It is noted that, prior to the light illumination, the 1 h adsorption testing without light already showed clearly remarkably reduced concentration of methylene blue in the solution containing TiO₂-OLC sample. Adsorption is very essential for photocatalysis, because it is the first stage of photocatalysis process to realize intimate contact between photocatalyst and pollutants. The enhanced adsorption for the OLC-containing coating is not surprising, since

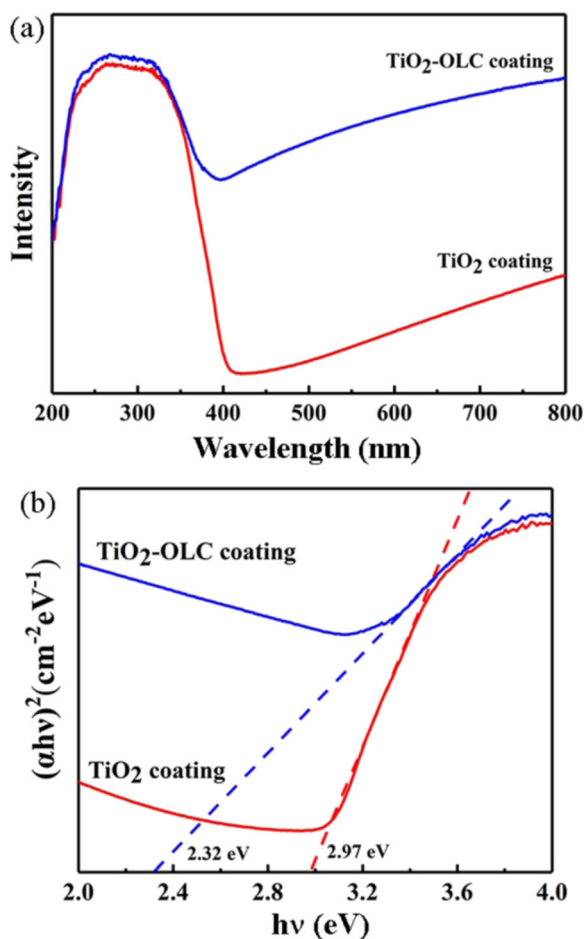


Fig. 6 UV-Vis spectra of the coatings. PL spectra (a) and Tauc plot (b) of the coatings

adsorption capacity is one of the amazing properties of carbon nanomaterials (Ko et al. 2016;

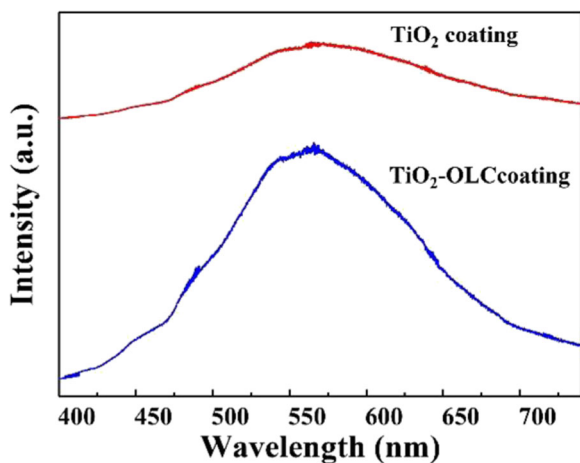


Fig. 7 Photoluminescence (PL) spectra under 325 nm excitation

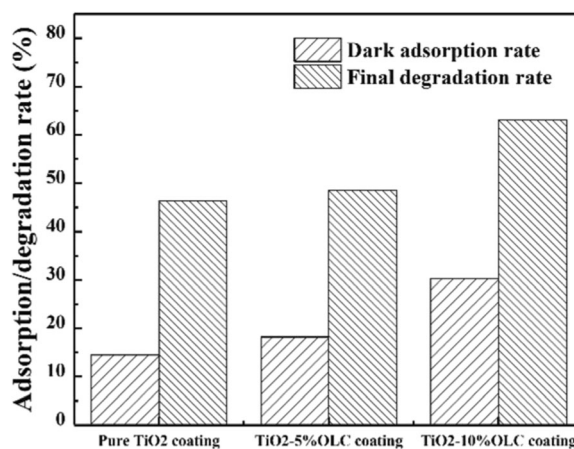


Fig. 8 The relationship between the dark adsorption rate and the final degradation rate

Sakulthaew et al. 2015; Seymour et al. 2012). Photocatalytic degradation of methylene blue usually follows Langmuir-Hinshelwood first-order kinetic equation (Xu et al. 2011). The kinetic model equation, $-\ln(C_t/C_0) = k \times t$, can be inferred from the degradation curves, where C_t and C_0 are the real-time and initial-time methylene blue concentration, respectively; t is reaction time; and k is the rate constant representing photocatalytic degradation rate reflected in the slope of the $-\ln(C_t/C_0)$ versus time curve. Obviously, the rate constant for TiO₂-OLC coating is higher than that for pure TiO₂ tested under illumination of both UV-light (Fig. 5b) and visible light (Fig. 5d).

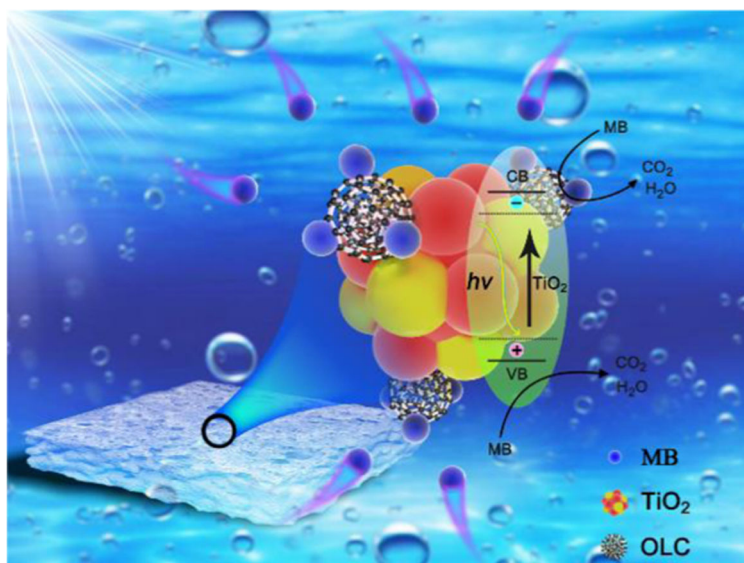
Mechanism of the enhanced performance

There are three key processes in the photocatalytic degrading of methylene blue, namely (i) absorption of photons to create electron-hole pairs, (ii) separation and migration/recombination of the photo-induced electron-hole pairs, and (iii) photocatalytic reaction on the photocatalyst surface. Hence, there are three corresponding key factors for enhanced photocatalytic performance, namely, reduced bandgap, reduced recombination rate of photo-induced carriers, and enhanced adsorption capacity towards pollutants.

Reduced bandgap

The primary factor influencing the photocatalytic activity is the bandgap of the semiconductor photocatalyst. To elucidate the sensitivity of

Fig. 9 Schematic diagram of photocatalytic enhancement mechanism



photocatalyst towards photon to create electron-hole pairs on the photocatalyst, the bandgap of both the coatings was examined. Under the UV-visible light illumination, for the OLC-containing coating, a distinct red shift in the adsorption edge and strong absorption in the visible light range was seen (Fig. 6a). Figure 6 b shows the curves of Kubelka-Munk remission function ($[\alpha hv]^{1/2}$ versus photon energy) corresponding to each spectrum, suggesting that the bandgap of the pure TiO_2 was 2.97 eV, while the bandgap of the OLC-containing coating was significantly reduced to 2.32 eV. The narrowing of the bandwidth is presumably attributed to the doping of OLC nanoparticles. The extended light absorption range for the TiO_2 -OLC coating could also account for the enhanced photocatalytic activities shown in Fig. 5. Similar band gap narrowing phenomenon of TiO_2 was also found in the case of TiO_2 -graphene composites, which could be attributed to the chemical bonding between TiO_2 and the specific sites of carbon. Nevertheless, the unpaired π electrons of OLC could easily bond with free titanium atoms on the surface of TiO_2 (Lee et al. 2012; Zhang et al. 2010d). As a result, the valence band edge was shifted, and the band gap was in turn reduced, which promotes the adsorption capacity of photons to create electron-hole pairs on the photocatalyst. And Fig. 9 shows the schematic diagram of the reduction of the bandgap.

Reduced recombination of photo-induced carriers

Photoluminescence (PL) emission spectroscopy provides an effective method to measure the irradiative recombination of electrons and holes, which is useful to elucidate the migration and separation rate of photo-induced carriers in photocatalysts. We therefore measured the PL spectra for both as-sprayed coatings (Fig. 7). Compared to pure TiO_2 , the PL emission intensity of TiO_2 -OLC coating is much lower, indicating that increased charge separation and transfer occur in OLC containing coating.

Enhanced adsorption capacity

Another key factor influencing the photocatalytic activity is the adsorption capacity of the semiconductor photocatalyst (Leary and Westwood 2011) towards pollutant molecules. In the previous study, various methods have been attempted to enhance the adsorption capacity of the photocatalyst, such as introducing suitable active sites with co-catalysts, increasing surface area with high surface-area-to-volume ratio of nanosized particles, and combining with carbonaceous nanomaterials to form π - π interaction towards the aromatic dyes. The enhanced adsorption capacity of the OLC-containing coating is likely responsible for the significantly accelerated degradation of methylene blue. Figure 8 shows the relationship between the dark adsorption rate and final degradation rate. It was noted that

the dark adsorption rate has been increased with the percentage of OLC increased from 0 to 10%, and the final degradation rate has been increased with the dark adsorption rate increased in this range. It has been well established that the adsorption is promoted by the π - π interaction between methylene blue and the aromatic regions of OLC, which is similar to the conjunction of methylene blue with graphene (Fan et al. 2012) and carbon nanotube (Ai et al. 2011). The specific interaction between OLC and methylene blue will promote the adsorption capacity of OLC-containing coating than pure TiO₂, which will accelerate the photocatalytic degrading activity. And Fig. 9 shows the schematic diagram of the enhanced adsorption capacity.

Conclusions

In summary, TiO₂-OLC coatings with uniformly distributed OLC nanoparticles and enhanced photocatalytic performances have been successfully fabricated via suspension plasma spray (SPS). The as-sprayed TiO₂-OLC coating showed remarkably enhanced performance as compared to the pure TiO₂ under both UV and visible light irradiation. The SPS processing gave rise to well retained physicochemical properties of TiO₂ and OLC in the binary coatings. And three aspects of the photocatalytic performance enhancement mechanism have been elucidated. The results would open a new window for designing and fabricating carbonaceous nanomaterial-doped TiO₂ coatings for photocatalytic applications.

Funding information This work was supported by Key Research and Development Program of Zhejiang Province (grant # 2017C01003), National Natural Science Foundation of China (grant # 41476064 and 31500772), and Zhejiang Provincial Natural Science Foundation of China (grant # LY18C100003).

Compliance with ethical standards

Conflict of interest The authors declare that they have no conflict of interest.

References

- Ai L, Zhang C, Liao F, Wang Y, Li M, Meng L, Jiang J (2011) Removal of methylene blue from aqueous solution with magnetite loaded multi-wall carbon nanotube: kinetic, isotherm and mechanism analysis. *J Hazard Mater* 198:282–290. <https://doi.org/10.1016/j.jhazmat.2011.10.041>
- Bannier E, Darut G, Sánchez E, Denoirjean A, Bordes MC, Salvador MD, Rayón E, Ageorges H (2011) Microstructure and photocatalytic activity of suspension plasma sprayed TiO₂ coatings on steel and glass substrates. *Surf Coat Technol* 206:378–386. <https://doi.org/10.1016/j.surfcoat.2011.07.039>
- Berman D, Narayanan B, Cherukara MJ, Sankaranarayanan S, Erdemir A, Zinovev A, Sumant AV (2018) Operando tribochemical formation of onion-like-carbon leads to macroscale superlubricity. *Nat Commun* 9:1164. <https://doi.org/10.1038/s41467-018-03549-6>
- Boningari T, Inturi SNR, Suidan M, Smimiotis PG (2018) Novel one-step synthesis of nitrogen-doped TiO₂ by flame aerosol technique for visible-light photocatalysis: effect of synthesis parameters and secondary nitrogen (N) source. *Chem Eng J* 350:324–334. <https://doi.org/10.1016/j.cej.2018.05.122>
- Chen Q, Tong RF, Chen XJ, Xue YK, Xie ZX, Kuang Q, Zheng LS (2018) Ultrafine ZnO quantum dot-modified TiO₂ composite photocatalysts: the role of the quantum size effect in heterojunction-enhanced photocatalytic hydrogen evolution. *Catal Sci Technol* 8:1296–1303. <https://doi.org/10.1039/c7cy02310c>
- Correia FC, Calheiros M, Marques J, Ribeiro JM, Tavares CJ (2018) Synthesis of Bi₂O₃/TiO₂ nanostructured films for photocatalytic applications. *Ceram Int* 44:22638–22644. <https://doi.org/10.1016/j.ceramint.2018.09.040>
- Fan LL, Luo CN, Li XJ, Lu FG, Qiu HM, Sun M (2012) Fabrication of novel magnetic chitosan grafted with graphene oxide to enhance adsorption properties for methyl blue. *J Hazard Mater* 215:272–279. <https://doi.org/10.1016/j.jhazmat.2012.02.068>
- Feng F, Yang WY, Gao S, Sun CX, Li Q (2018) Postillumination activity in a single-phase photocatalyst of Mo-doped TiO₂ nanotube array from its photocatalytic “memory”. *ACS Sustain Chem Eng* 6:6166–6174. <https://doi.org/10.1021/acssuschemeng.7b04845>
- Fitri MA, Ota M, Hirota Y, Uchida Y, Hara K, Ino D, Nishiyama N (2017) Fabrication of TiO₂-graphene photocatalyst by direct chemical vapor deposition and its anti-fouling property. *Mater Chem Phys* 198:42–48. <https://doi.org/10.1016/j.matchemphys.2017.05.053>
- Ghosh M, Sonkar SK, Saxena M, Sarkar S (2011) Carbon nanonions for imaging the life cycle of drosophila melanogaster. *Small*. 7:3170–3177. <https://doi.org/10.1002/sml.201101158>
- Hao RR, Wang GH, Jiang CJ, Tang H, Xu QC (2017) In situ hydrothermal synthesis of g-C₃N₄/TiO₂ heterojunction photocatalysts with high specific surface area for Rhodamine B degradation. *Appl Surf Sci* 411:400–410. <https://doi.org/10.1016/j.apsusc.2017.03.197>
- Kho YK, Iwase A, Teoh WY, Maedler L, Kudo A, Amal R (2010) Photocatalytic H₂ evolution over TiO₂ nanoparticles: the synergistic effect of anatase and rutile. *J Phys Chem C* 114:2821–2829. <https://doi.org/10.1021/jp910810r>
- Ko YJ, Choi K, Lee S, Cho JM, Choi HJ, Hong SW, Choi JW, Mizuseki H, Lee WS (2016) Chromate adsorption mechanism on nanodiamond-derived onion-like carbon. *J Hazard*

- Mater 320:368–375. <https://doi.org/10.1016/j.jhazmat.2016.08.041>
- Kuznetsov VL, Chuvilin AL, Butenko YV, Malkov IY, Titov VM (1994) Onion-like carbon from ultra-disperse diamond. *Chem Phys Lett* 222:343–348. [https://doi.org/10.1016/0009-2614\(94\)87072-1](https://doi.org/10.1016/0009-2614(94)87072-1)
- Leary R, Westwood A (2011) Carbonaceous nanomaterials for the enhancement of TiO₂ photocatalysis. *Carbon*. 49:741–772. <https://doi.org/10.1016/j.carbon.2010.10.010>
- Lee JS, You KH, Park CB (2012) Highly photoactive, low bandgap TiO₂ nanoparticles wrapped by graphene. *Adv Mater* 24:1084–1088. <https://doi.org/10.1002/adma.201104110>
- Li X, Yu JG, Wageh S, Al-Ghamdi AA, Xie J (2016) Graphene in photocatalysis: a review. *Small*. 12:6640–6696. <https://doi.org/10.1002/sml.201600382>
- Li X, Yu J, Li G, Liu H, Wang A, Yang L, Zhou W, Chu B, Liu S (2018) TiO₂ nanodots anchored on nitrogen-doped carbon nanotubes encapsulated cobalt nanoparticles as photocatalysts with photo-enhanced catalytic activity towards the pollutant removal. *J Colloid Interface Sci* 526:158–166. <https://doi.org/10.1016/j.jcis.2018.04.102>
- Liu G, Yang HG, Pan J, Yang YQ, Lu GQ, Cheng H-M (2014) Titanium dioxide crystals with tailored facets. *Chem Rev* 114:9559–9612. <https://doi.org/10.1021/cr400621z>
- Liu H, Chen Z, Zhang L, Zhu D, Zhang Q, Luo Y, Shao X (2018) Graphene grown on anatase-TiO₂ nanosheets: enhanced photocatalytic activity on basis of a well-controlled interface. *J Phys Chem C* 122:6388–6396. <https://doi.org/10.1021/acs.jpcc.7b12305>
- Nalid NR, Majid A, Tahir MB, Niaz NA, Khalid S (2017) Carbonaceous-TiO₂ nanomaterials for photocatalytic degradation of pollutants: a review. *Ceram Int* 43:14552–14571. <https://doi.org/10.1016/j.ceramint.2017.08.143>
- Pawlowski L (2009) Suspension and solution thermal spray coatings. *Surf Coat Technol* 203:2807–2829. <https://doi.org/10.1016/j.surfcoat.2009.03.005>
- Rajagopal R, Ryu K-S (2018) Synthesis of rGO-doped Nb₄O₅-TiO₂ nanorods for photocatalytic and electrochemical energy storage applications. *Appl Catal B* 236:125–139. <https://doi.org/10.1016/j.apcatb.2018.03.112>
- Re M, Liu H, Qu J, Zhang Y, Ma Y, Yuan X (2018) The different paths and potential risks of photo(-electro)-catalytic degradation for rhodamine B in water by graphene/TiO₂ membrane. *Environ Sci Pollut Res* 25:13988–13999. <https://doi.org/10.1007/s11356-018-1611-4>
- Ren K, Liu Y, He X, Li H (2015) Suspension plasma spray fabrication of nanocrystalline titania hollow microspheres for photocatalytic applications. *J Therm Spray Technol* 24:1213–1220. <https://doi.org/10.1007/s11666-015-0296-1>
- Robinson BW, Tighe CJ, Guarr RI, Mills A, Parkin IP, Tabecki AK, de Villiers Lovelock HL, Darr JA (2015) Suspension plasma sprayed coatings using dilute hydrothermally produced titania feedstocks for photocatalytic applications. *J Mater Chem A* 3:12680–12689. <https://doi.org/10.1039/c4ta05397d>
- Sakthivel S, Shankar MV, Palanichamy M, Arabindoo B, Bahnemann DW, Murugesan V (2004) Enhancement of photocatalytic activity by metal deposition: characterisation and photonic efficiency of Pt, Au and Pd deposited on TiO₂ catalyst. *Water Res* 38:3001–3008. <https://doi.org/10.1016/j.watres.2004.04.046>
- Sakulthaew C, Comfort SD, Chokeyaroenrat C, Li X, Harris CE (2015) Removing PAHs from urban runoff water by combining ozonation and carbon nano-onions. *Chemosphere*. 141:265–273. <https://doi.org/10.1016/j.chemosphere.2015.08.002>
- Schneider J, Matsuoka M, Takeuchi M, Zhang J, Horiuchi Y, Anpo M, Bahnemann DW (2014) Understanding TiO₂ photocatalysis: mechanisms and materials. *Chem Rev* 114:9919–9986. <https://doi.org/10.1021/cr5001892>
- Seymour MB, Su C, Gao Y, Lu Y, Li Y (2012) Characterization of carbon nano-onions for heavy metal ion remediation. *J Nanopart Res* 14. <https://doi.org/10.1007/s11051-012-1087-y>
- Shaban M, Ashraf AM, Abukhadra MR (2018) TiO₂ nanoribbons/carbon nanotubes composite with enhanced photocatalytic activity: fabrication, characterization, and application. *Sci Rep* 8:781. <https://doi.org/10.1038/s41598-018-19172-w>
- Toma FL, Bertrand G, Begin S, Meunier C, Barres O, Klein D, Coddet C (2006a) Microstructure and environmental functionalities of TiO₂-supported photocatalysts obtained by suspension plasma spraying. *Appl Catal B* 68:74–84. <https://doi.org/10.1016/j.apcatb.2006.07.009>
- Toma FL, Bertrand G, Chwa SO, Meunier C, Klein D, Coddet C (2006b) Comparative study on the photocatalytic decomposition of nitrogen oxides using TiO₂ coatings prepared by conventional plasma spraying and suspension plasma spraying. *Surf Coat Technol* 200:5855–5862. <https://doi.org/10.1016/j.surfcoat.2005.08.148>
- Toma FL, Bertrand G, Klein D, Coddet C, Meunier C (2006c) Nanostructured photocatalytic titania coatings formed by suspension plasma spraying. *J Therm Spray Technol* 15:587–592. <https://doi.org/10.1361/105996306x147234>
- Tomaszek R, Pawlowski L, Gengembre L, Laureyns J, Znamirovski Z, Zdanowski J (2006) Microstructural characterization of plasma sprayed TiO₂ functional coating with gradient of crystal grain size. *Surf Coat Technol* 201:45–56. <https://doi.org/10.1016/j.surfcoat.2005.10.033>
- Ton NNT, Dao ATN, Kato K, Ikenaga T, Trinh DX, Taniike T (2018) One-pot synthesis of TiO₂/graphene nanocomposites for excellent visible light photocatalysis based on chemical exfoliation method. *Carbon*. 133:109–117. <https://doi.org/10.1016/j.carbon.2018.03.025>
- Ugarte D (1992) Curling and closure of graphitic networks under electron-beam irradiation. *Nature*. 359:707–709. <https://doi.org/10.1038/359707a0>
- Wang Z, Lang XJ (2018) Visible light photocatalysis of dye-sensitized TiO₂: the selective aerobic oxidation of amines to imines. *Appl Catal B* 224:404–409. <https://doi.org/10.1016/j.apcatb.2017.10.002>
- Wang R, Lu KQ, Tang ZR, Xu YJ (2017) Recent progress in carbon quantum dots: synthesis, properties and applications in photocatalysis. *J Mater Chem A* 5:3717–3734. <https://doi.org/10.1039/c6ta08660h>
- Woan K, Pyrgiotakis G, Sigmund W (2009) Photocatalytic carbon-nanotube-TiO₂ composites. *Adv Mater* 21:2233–2239. <https://doi.org/10.1002/adma.200802738>
- Xu J, Chen M, Fu D (2011) Study on highly visible light active Bi-doped TiO₂ composite hollow sphere. *Appl Surf Sci* 257:7381–7386. <https://doi.org/10.1016/j.apsusc.2011.02.030>

- Zeiger M, Jackel N, Asian M, Weingarth D, Presser V (2015) Understanding structure and porosity of nanodiamond-derived carbon onions. *Carbon*. 84:584–598. <https://doi.org/10.1016/j.carbon.2014.12.050>
- Zeiger M, Jackel N, Mochalin VN, Presser V (2016) Review: carbon onions for electrochemical energy storage. *J Mater Chem A* 4:3172–3196. <https://doi.org/10.1039/c5ta08295a>
- Zhang X-Y, Li H-P, Cui X-L, Lin Y (2010a) Graphene/TiO₂ nanocomposites: synthesis, characterization and application in hydrogen evolution from water photocatalytic splitting. *J Mater Chem* 20:2801–2806. <https://doi.org/10.1039/b917240h>
- Zhang H, Lv X, Li Y, Wang Y, Li J (2010b) P25-graphene composite as a high performance photocatalyst. *ACS Nano* 4:380–386. <https://doi.org/10.1021/nn901221k>
- Zhang YH, Tang ZR, Fu XZ, Xu YJ (2010c) TiO₂-graphene nanocomposites for gas-phase photocatalytic degradation of volatile aromatic pollutant: is TiO₂-graphene truly different from other TiO₂-carbon composite materials? *ACS Nano* 4: 7303–7314. <https://doi.org/10.1021/nn1024219>
- Zhang JL, Wu YM, Xing MY, Leghari SAK, Sajjad S (2010d) Development of modified N doped TiO₂ photocatalyst with metals, nonmetals and metal oxides. *Energy Environ Sci* 3: 715–726. <https://doi.org/10.1039/b927575d>

Publisher's note Springer Nature remains neutral with regard to jurisdictional claims in published maps and institutional affiliations.